

Extrinsic Effects in the Dynamics and Selection of Cellular Arrays

B. Billia,* H. Jamgotchian,† and H. Nguyen Thi‡
Université d'Aix-Marseille, 13397 Marseille Cedex 20, France
P. Cerisier§
Université d'Aix-Marseille I, 13397 Marseille Cedex 20, France
and
R. Trivedi¶
Iowa State University, Ames, Iowa 50011

In addition to convection in the liquid phase, which can be made negligible in microgravity, other extrinsic effects should be suppressed, or at least controlled, in order to be able to actually relate the dynamics and selection of cellular arrays that result from the pure morphological instability of a planar solidification front to the processing parameters: growth velocity V , thermal gradient G , and solute concentration C_0 . Therefore, we successively analyzed the influence of four major extrinsic sources of "parasitic" effects in cellular solidification and, when complementary, in Bénard convection with a free surface. The container imposes confinement and wall conditions. Cellular doublets or spatiotemporal chaos are favored by the presence of grain boundaries. When the solute is volatile, gas pores may nucleate, which then provoke capillary convection and whose growth can either suppress morphological instability or form localized duplexes, upon coupling with a cellular or dendritic envelope. Finally, the experimental procedure, essentially through the initial conditions that are applied, determines the initial transient and sometimes prevents the asymptotic state to be reached, possibly by dynamically locking the system in an intermediate configuration, characterized by a significant amount of "noise."

Nomenclature

- C_0 = initial solute concentration
 d = container width
 G = thermal gradient
 L = solidified length
 m = average edge length of the minimal spanning tree
 V = growth velocity
 V_c = critical velocity for morphological instability of a planar solidification front
 ΔV = velocity gap (procedure 2 for directional solidification of Pb-30 wt% Ti alloys)
 $\Delta\lambda$ = standard deviation of primary spacing
 λ = cell size in an unconstrained medium (computed from linear stability analysis close to the threshold of instability or otherwise estimated in experiments in large containers)
 $\langle\lambda\rangle$ = average primary spacing

σ = standard deviation of the minimal spanning tree edge-length distribution

Introduction

SINCE it allows a close control of the solid microstructure, and thus of the properties of the material, controlled solidification is a major technique to produce engineering components. Consequently, it is important to establish the precise correlation between the microstructure and the processing conditions. Furthermore, in the last years interesting similarities have been appreciated between several pattern-forming instabilities in different fields of science,^{1–3} which led to significant theoretical advances in the understanding of the selection and stability of structures. Cells and dendrites, which result from morphological instabilities of the solidification front, belong to this family. Therefore, besides their long-time known technological importance, these nonlinear patterns have now gained further attention as archetypes. In particular, the question of the ultimate selection of the primary spacing is most intriguing for the physicist seeking for the various ways in which the selection of cellular pattern may or may not occur.¹ This article concerns the influence of extrinsic effects on the dynamics and selection of cellular arrays (Fig. 1). Although our main interest is the cellular directional solidification of a binary alloy, Bénard cells (convection cells in a thin liquid layer with an upper free surface heated from below) will also be considered.

Indeed, as the minimal spanning tree (MST) contains all information on pattern organization and leads to a unique edge-length histogram, the statistical analysis of array arrangement by the MST method is meaningful.⁴ It follows^{2,3} that, in the (m, σ) diagram, the representative points fall on the trajectory joining the honeycomb to the random distribution for both solidification cells and Bénard cells (Fig. 2). This means that, despite a high percentage of defects, the underlying mosaic is still detectable. Basically, the cell centers form a triangular array, and the disorder associated to the

Received Nov. 23, 1992; presented as Paper 93-0264 at the AIAA 31st Aerospace Sciences Meeting and Exhibit, Reno, NV, Jan. 11–14, 1993; revision received March 1, 1993; accepted for publication March 2, 1993. Copyright © 1993 by the American Institute of Aeronautics and Astronautics, Inc. All rights reserved.

*Research Director, Head of Department, Laboratoire MATériaux: Organisation et Propriétés (ERS CNRS no. 14), Faculté des Sciences de St. Jérôme, Case 151. Member AIAA.

†Senior Scientist, Laboratoire MATériaux: Organisation et Propriétés (ERS CNRS no. 14), Faculté des Sciences de St. Jérôme, Case 151.

‡Assistant Professor of Physics, Laboratoire MATériaux: Organisation et Propriétés (ERS CNRS no. 14), Faculté des Sciences de St. Jérôme, Case 151.

§Professor of Physics, IUSTI (URA CNRS no. 1168), Faculté des Sciences de St. Jérôme, Case 162.

¶Senior Scientist and Professor of Materials Science and Engineering, Ames Laboratory USDOE and Department of Materials Science and Engineering.

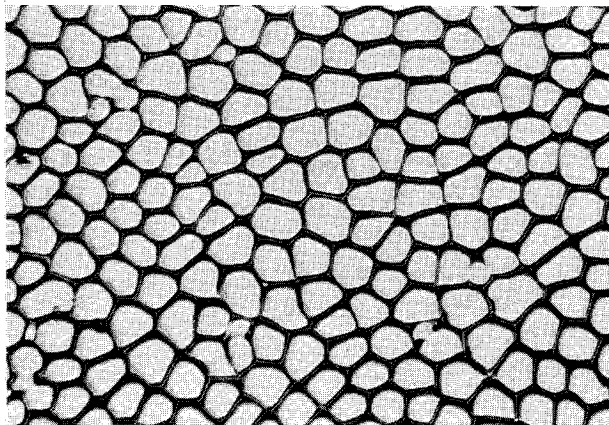


Fig. 1 Cellular array in upward solidification of a Pb-30 wt % Ti alloy. $G = 45^\circ\text{C}/\text{cm}$, $V = 1.1 \text{ cm/h}$. Chemical etching on a transverse section. Image width = 3.2 mm.

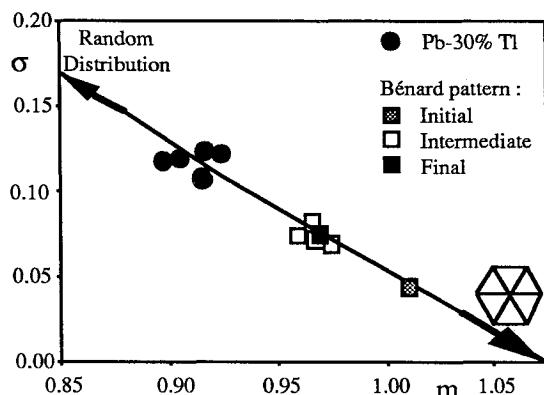


Fig. 2 Representative points in the (m, σ) diagram for arrays of solidification cells in Pb-30 wt % Ti alloys and for the time evolution of a Bénard pattern.

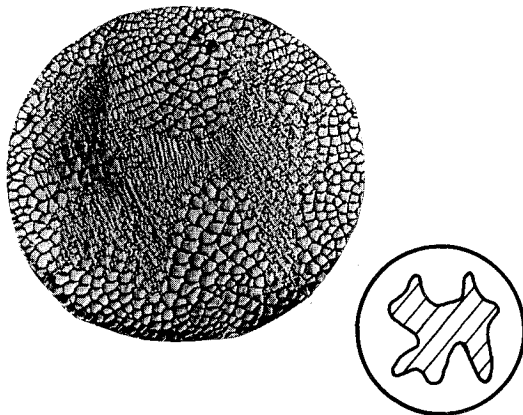


Fig. 3 Effect of a macroscopic modulation of the solid-liquid interface (solid plateaus on the periphery are separated by a depletion filled with quenched liquid, hatched area) on the regularity of the cellular array. Pb-30 wt % Ti, $G = 55^\circ\text{C}/\text{cm}$, $V = 2 \text{ cm/h}$. Sample diameter = 4 mm. Chemical etching on a transverse section.

topological defects can be described by the superposition of a Gaussian "noise." Therefore, we believe that the simultaneous and complementary investigation of different systems is likely to provide critical information on morphogenesis in honeycomb-forming instabilities. In particular, it would be worthwhile to determine if the relation "cellular array = honeycomb + Gaussian noise" is a generic feature and to search for the physical origin of this noise. In order to achieve these goals and actually relate the dynamics and selection of cellular arrays to the sole processing parameters, namely V ,

G , and C_0 in directional solidification, one should first get rid of, or at least control, all extrinsic effects.

Convection in the liquid phase, which on the ground distorts the macroscopic shape of the solidification front^{5,6} and makes the level of morphological instability nonhomogeneous (Fig. 3), can be made negligible in microgravity. In the following, we will successively analyze the influence of four major extrinsic sources of parasitic effects: 1) the crucible, or container; 2) the grain boundaries; 3) the gas pores; and 4) the experimental procedure, essentially through the initial conditions that are applied.

Container

The crucible, or container, imposes confinement and wall conditions. To be active on structure formation and selection, lateral constraints must be at the scale of the primary spacing,⁷ otherwise, only the cells on the periphery are altered to match with the boundaries. The parameter that dictates the large or small size of the container is the ratio d/λ . For instance, in Bénard convection in small vessels, a cell can be imposed in the center⁸ which relaxes towards the unit hexagonal cell surrounded by six half-cells for d/λ about two (Fig. 4). Such information on the adaptation to a very restricted environment and the entrance of the hexagonal array should prove useful in the understanding of cellular solidification in a capillary or an interstice.

The influence of lateral confinement also very much depends on the compatibility of the geometry of the cellular array with the geometry of the container. In a square vessel, there can be only two compatible walls for Bénard cells, i.e., perpendicular to the boundaries of hexagonal border cells. Then, array disorder first appears at the two incompatible walls, which are set vertical in Fig. 5.

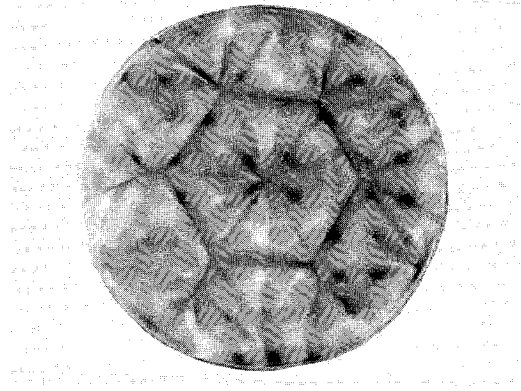


Fig. 4 Hexagonal Bénard cell centered in a cylindrical container of 13.5 cm in diameter.

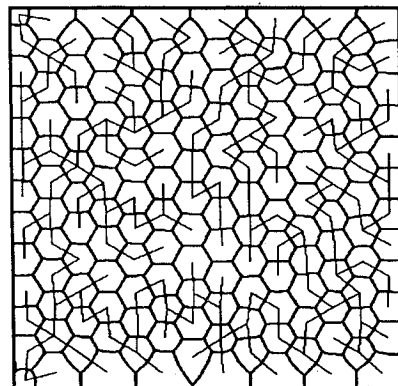


Fig. 5 Birth of topological disorder from the incompatible walls of a square vessel with 25-cm sides, 10 min after the initial imposition of a perfect array of Bénard cells possessing walls perpendicular to the vertical sides. Binary image with MST.

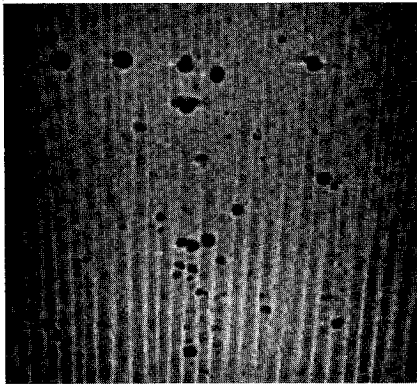


Fig. 6 Outward drift of the cell walls due to cell advection along the convex solid-liquid interface. Pb-30 wt % Tl solidified in microgravity. $V = 0.7$ cm/h, $G = 20^\circ\text{C}/\text{cm}$. Sample diameter = 9.5 mm. Chemical etching on a longitudinal section.

In solidification experiments, wall conditions are often dominant. For Pb-Tl alloys, the phase boundary is macroscopically convex due to the difference in thermal conductivity between liquid and solid, as shown under diffusive conditions in the D1 mission.⁹ It follows that the cells are advected from the center towards the periphery as revealed by the curved trajectories of the cell walls in Fig. 6. Consequently, there should be a continuous creation of new cells in the central part of the sample. The serious drawback then is that the curvature of the front is a permanent source of array dynamics, which would impede the system to reach a true steady state.

Grain Boundaries

Although the preferential coupling between morphological instability and grain boundaries has long been recognized, in cellular growth, the grain boundaries are essentially considered as artifacts to be buried in the intercellular grooves. Nevertheless, observations on succinonitrile-acetone alloys show that this is a much too restricted vision. Indeed, the pairs of asymmetric cells that develop at grain boundaries can duplicate within the grains (Fig. 7) eventually resulting, after complete invasion and cell eliminations, in a stable doublet microstructure (Fig. 8).

The range of stability of doublets is found to be narrow,¹⁰ roughly in the regime where finite amplitude cells transform to deep cells. Observations show that whether an interface with a doublet formation is stable or not depends upon the stability against the tip-splitting phenomenon. In the unstable case, the nonlinear dynamics give rise to a cellular array (Fig. 9). After initial perturbations, the wavelength selection process begins with cell elimination (Fig. 9a), which causes the neighboring cells to enlarge. However, instead of forming a doublet, these coupled cells undergo the tip-splitting process at the time they become too large, which in a first approximation induces a halving of the local spacing. This perturbation in local spacing then is propagated laterally along the array, which provokes cell elimination (Fig. 9b). This halving enables the cells on both sides of the grain boundary to recommence there the building of a doublet which, as before, is doomed to failure. As such a sequence is self-sustained in places where there are grain boundaries, it follows that the grain boundaries are the principal source of spatiotemporal chaos which prevents a steady state to be achieved in the pattern (Fig. 9c).

Besides, grain boundaries can be seen as a means of introducing lateral constraints possessing their own specific dynamics that must couple with the dynamics of the interface microstructure. For instance, grain boundaries are able to shift laterally in order to accommodate the doublet microstructure (Fig. 10).

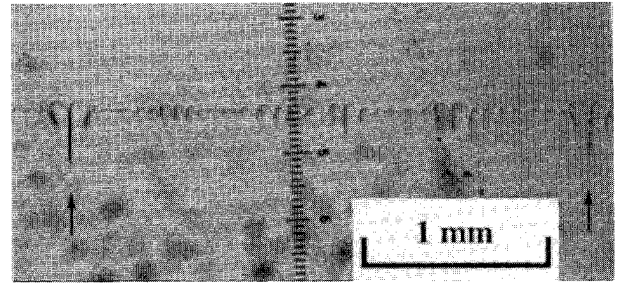


Fig. 7 Progressive initiation of coupled cells within a large grain and lateral propagation of morphological instability in the form of wave packets. Succinonitrile-0.5 wt % acetone, $V = 1$ $\mu\text{m}/\text{s}$, $G = 30^\circ\text{C}/\text{cm}$. Grain boundaries are indicated by arrows.

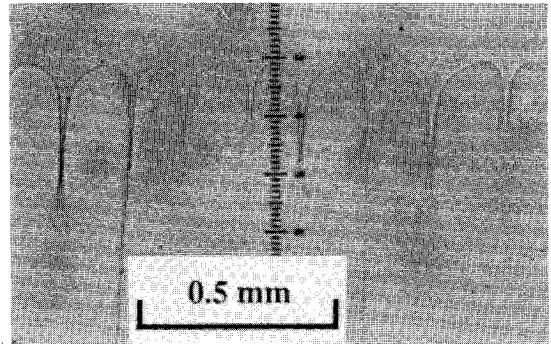


Fig. 8 Stable array of cellular doublets formed after 11,280 s of growth. Succinonitrile-0.5 wt % acetone, $V = 0.75$ $\mu\text{m}/\text{s}$, $G = 43^\circ\text{C}/\text{cm}$.

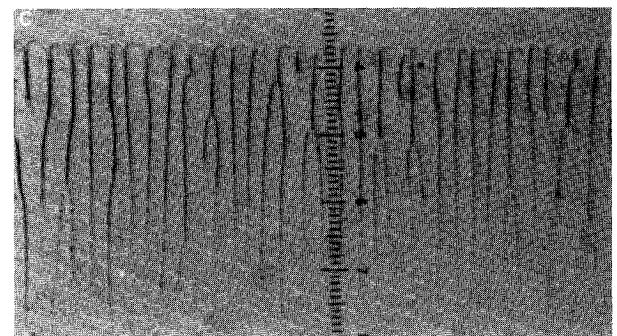
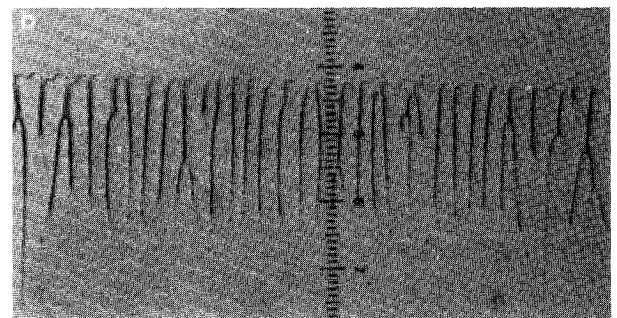
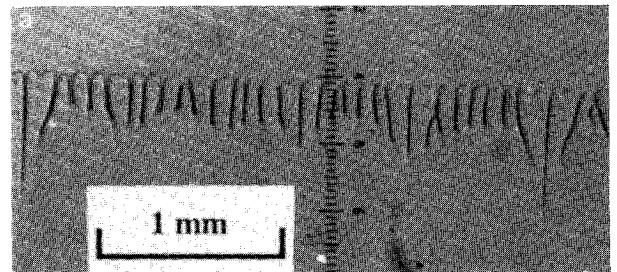


Fig. 9 Evolution of a cellular pattern above the range of stable doublet growth. Succinonitrile-0.5 wt % acetone, $V = 1$ $\mu\text{m}/\text{s}$, $G = 30^\circ\text{C}/\text{cm}$. Patterns formed after a) 2700 s, b) 3600 s, and c) 4500 s.

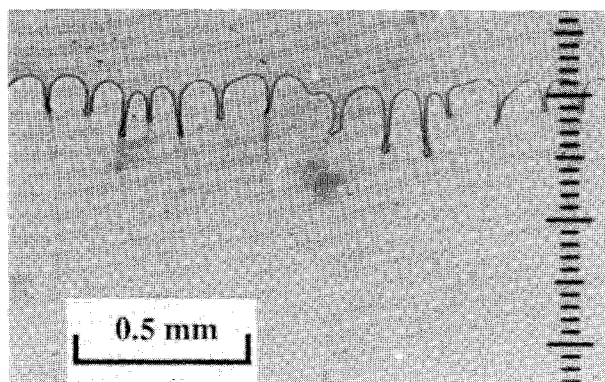


Fig. 10 Lateral motion of grain boundaries to match the width of the grain to the doublet array. Succinonitrile-0.5 wt % acetone, $V = 0.75 \mu\text{m/s}$, $G = 43^\circ\text{C/cm}$.

Gas Pores

When solute is volatile, as acetone is in succinonitrile, bubbles can form in directional solidification of a binary alloy even starting from extremely pure materials. Bubbles commonly nucleate well ahead of the solid-liquid interface which, while being pushed or captured, greatly alter the front microstructure, introducing changes in primary spacing and array disorder (Fig. 11).

More often, bubbles nucleate in the intercellular grooves that are enriched in acetone. These bubbles either get trapped or detach and migrate to the level of the tips, where they coarsen, become elongated, and create cylindrical inclusions when captured. Another type of interface microstructure, localized duplexes, can also develop upon the formation of solid sheaths around the elongated bubbles (Fig. 12). As a bubble is a sink for acetone and the solidification front a source, there is a source-sink competition which, with the interplay of capillary convection driven by gradients of surface tension at the gas-liquid interface (bubble cap), leads to the formation of an internal oscillator, whose frequencies can be determined from the fast Fourier transform of the time variation of the bubble diameter.¹¹

Possessing a rich and complex dynamical behavior, duplexes strongly effect the solidification microstructure in their neighborhood. Cellular duplexes disrupt the solidification front and either partly superpose on, or readily incorporate into, the cellular array. Dendritic duplexes, undergoing coherent side-branching, are observed when the level of morphological instability is increased (Fig. 13). In contrast to the usual dendritic side-branching induced by experimental broadband or white noise, coherent side-branching on a dendritic duplex results from selective amplification in the discrete spectrum of frequencies generated by the internal oscillator. In the linear region of amplification, the dominant frequency is the closest to maximum amplification in the continuous band of unstable frequencies obtained by local application of linear analysis of morphological instability of a planar front.¹¹ A striking feature certainly is that the side-branches then remain symmetrical, even in the highly nonlinear regime.

It should be noticed that the absorption of acetone by the bubble creates a lateral gradient of solute or, in other words, a ramp in the level of morphological instability. When a planar-cellular transition is induced along the interface, the primary spacing is more able to adjust by the lateral motion mechanism.¹²

Experimental Procedure

In order to analyze the influence of the initial transient on the formation of a cellular array, two series of experiments were carried out on Pb-30 wt % Tl alloys using different procedures. In the first series, the system is initially solidified at a velocity of 0.4 cm/h which is below the critical velocity previously determined, $V_c = 0.60 \text{ cm/h}$. Once steady-state

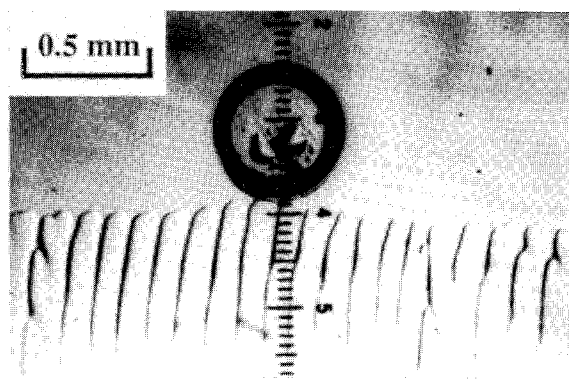


Fig. 11 Blocking of cells in the beginning of bubble engulfment in the solid. Succinonitrile-0.5 wt % acetone, $V = 1 \mu\text{m/s}$, $G = 30^\circ\text{C/cm}$.

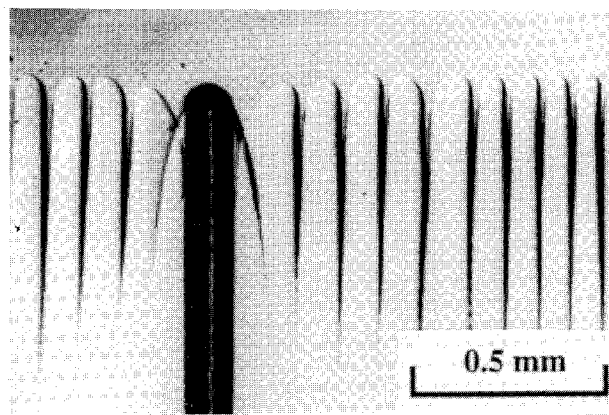


Fig. 12 Localized cellular duplex within an array of deep cells. Succinonitrile-0.15 wt % acetone, $V = 4 \mu\text{m/s}$, $G = 65^\circ\text{C/cm}$.

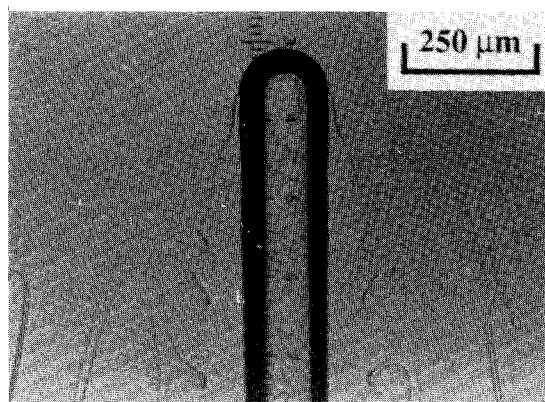


Fig. 13 Coherent side-branching on dendritic duplex. Succinonitrile-0.5 wt % acetone, $V = 2 \mu\text{m/s}$, $G = 30^\circ\text{C/cm}$.

planar growth is established, the furnace velocity is suddenly driven at a velocity of 0.85 cm/h which corresponds to cellular growth. The response of the solid-liquid interface to the application of ΔV is then examined. With the second procedure, the velocity of cellular growth is applied from the very beginning of solidification. It is then possible to study the evolution of the cellular patterns towards the steady-state array. In both cases, solidification is stopped by quenching the sample after different durations at 0.85 cm/h. The morphology of the solidification front is therefore frozen, which enables the study of the interface microstructure vs L .⁵

By using the weighted Wigner-Seitz construction,² $\langle \lambda \rangle$ and $\Delta \lambda$ are measured for each cellular pattern (Fig. 14). With procedure 1, for a solidified length of 1 cm, the solid-liquid interface is dendritic (results are given for an orientation very

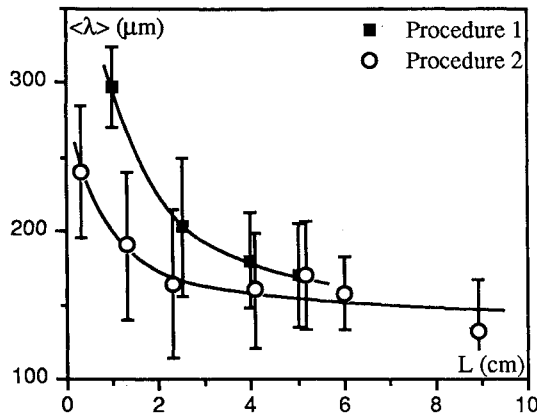


Fig. 14 Variation of the primary spacing $\langle \lambda \rangle$ vs solidified length L at $V = 0.85$ cm/h. Pb-30 wt % Tl, $G = 45^\circ\text{C}/\text{cm}$.

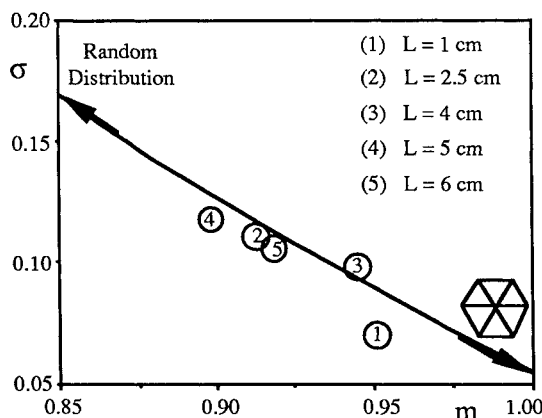


Fig. 15 Evolution in the (m, σ) diagram of the cellular array disorder with L . Pb-30 wt % Tl.

close to $\langle 100 \rangle$ as the pattern depends on growth axis). This means that the interface velocity significantly overshoots to compensate the initial inertia in the response to the variation ΔV in the furnace velocity. Then, the front velocity necessarily slows down so that the interface restabilizes into cells whose size decreases towards the asymptotic value. With procedure 2, the velocity overshoot is less pronounced so that, on the average, convergence is more rapid.

Detailed information on array disorder in the process of spacing adjustment is obtained by the MST method. In Fig. 15, one can see the evolution in the (m, σ) diagram when L is increased. Initially, the average cell size is too large so that cell divisions occur by tip-splitting or mitosis. This phase introduces a large number of defects so that m decreases while σ increases (Fig. 15: from 1 to 2). After this first stage, rearrangement follows during which both primary spacing and array disorder decrease (Fig. 15: from 2 to 3). The increase of m is due to the lowering of the number of very small cells, which preferentially contribute to the edge length histogram as they naturally provide short edges in the MST. Then, the process of cell division and rearrangement is repeated (respectively, from 3 to 4 and from 4 to 5 in Fig. 15), giving rise to an oscillatory approach of the asymptotic state, in the sense of disorder.

Whereas, in solidification experiments, it seems impossible to choose the initial conditions, i.e., the initial cellular array, in Bénard convection, the patterns can be carefully investigated either starting from the natural instability of the fluid layer¹³ or by using a thermal indentation technique to generate hexagonal cells with an imposed side.⁸ Using the former procedure, critical experiments have stressed that it is only after a very slow elimination of defects by pair annihilation in a transient, and also at the container wall, that the percentage

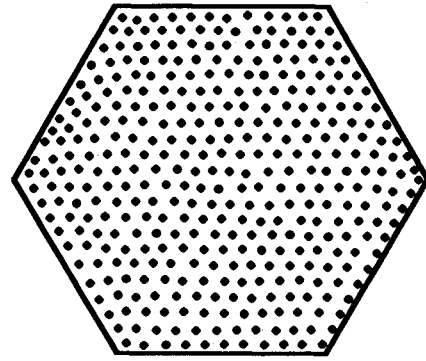


Fig. 16 Absence of disorder in the bulk array when a honeycomb with the natural spacing is initially imposed. Bénard cells. Hexagon side = 17 cm, distance from threshold = 4.5. Black dots correspond to cell centers.

of defects reaches a constant value, that is characteristic of and increases with the level of instability.¹³ The latter procedure enables one to start very close to the perfect hexagonal pattern and follow the representative point in the (m, σ) diagram (Fig. 2). Starting from an initial spacing lower than the steady-state one, cell eliminations first occur by which the average size increases rapidly towards its stationary value while increasing the level of disorder (Fig. 2), very much like solidification. But, unlike solidification, no visible oscillation or subsequent amelioration of the array is then observed. The final point for the Bénard array remains close to the data points for the Pb-30 wt % Tl alloys obtained by "standard" directional solidification, i.e., by suddenly switching the growth velocity on after thermal stabilization.

Obviously, the locking of a pattern in an intermediate configuration might be due to some time scale far exceeding the duration of the experiment. In that case, it would be hopeless to express the sharpness of selection in usual experiments in a limited time as a function of the control parameters only. Yet, other physical mechanisms are still conceivable that could introduce a significant amount of disorder, among which the dynamics of formation of the cellular array itself. Indeed, a critical experiment in Bénard convection, carried out by initially imposing a honeycomb with a spacing "adapted" to the level of instability, showed no array dynamics during four days, apart from the cells close to the container walls (Fig. 16). It followed that the cellular array remained perfect, without topological defects and disorder. Such an experiment suggests to conjecture that "no dynamics = no disorder," which will be ascertained in forthcoming studies.

Conclusions

Is primary spacing selection in cellular solidification a reality, an approximation, or a myth? A band of spacings, possibly narrow, is predicted by theories, but the possibilities of a dynamical or noise-driven selection are largely unexplored.¹ Therefore, a major conclusion of our studies certainly is that, for a meaningful analysis of the formation and sharpness of selection of cellular arrays in directional solidification, it is mandatory to separate the processes linked to the spreading and amplification of the interface perturbations and to the wavelength adjustment itself from the processes of extrinsic origins.

It is found that in cellular solidification the final state is the same for two common experimental procedures, independently of the transients. Nevertheless, although some insight has been gained in Bénard convection, the feasibility of an optimized directional solidification procedure, which would rapidly converge to the asymptotic state, still is an open question, in particular the artificial selection of an array with a unique spacing.

Finally, all the "parasitic" effects we have discussed are, by themselves, very appealing from a physicist point of view,

because the present understanding of their underlying mechanisms is relatively poor. Microgravity, by suppressing buoyancy convection in the melt, would also provide a unique way for studying pure phenomena.

Acknowledgments

This work was supported by the Centre National d'Etudes Spatiales and the Centre National de la Recherche Scientifique. A part was carried out at Ames Laboratory which is operated for the U.S. Department of Energy by Iowa State University under Contract W-7405-ENG-82. H. Jamgotchian benefited from a CNRS-NSF exchange, and B. Billia and R. Trivedi from a NATO Research Grant.

References

- ¹Langer, J. S., "Lectures in the Theory of Pattern Formation," *Proceedings of the 46th Les Houches Symposium on Chance and Matter*, edited by J. Souletie, J. Vannimenus, and R. Stora, Elsevier, Amsterdam, 1987, pp. 629-711.
- ²Billia, B., Jamgotchian, H., and Nguyen Thi, H., "Statistical Analysis of the Disorder of Two-Dimensional Cellular Arrays in Directional Solidification," *Metallurgical Transactions A*, Vol. 22, Dec. 1991, pp. 3041-3050.
- ³Cerisier, P., Nguyen Thi, H., and Billia, B., "Disorder Dynamics of Arrays in Bénard Convection," *Physica D*, Vol. 61, Dec. 1992, pp. 113-118.
- ⁴Dussert, C., Rasigni, G., Rasigni, M., Palmari, J. P., and Llebaria, A., "Minimal Spanning Tree: A New Approach for Studying Order and Disorder," *Physical Review B*, Vol. 34, Sept. 1986, pp. 3528-3531.
- ⁵Jamgotchian, H., Billia, B., and Capella, L., "Thermosolutal Convection-Induced Morphologies of the Solid-Liquid Interface During Upward Solidification of Pb-30 wt % Tl Alloys," *Journal of Crystal Growth*, Vol. 82, No. 3, 1987, pp. 342-350.
- ⁶Nguyen Thi, H., Billia, B., and Jamgotchian, H., "Influence of Thermosolutal Convection on the Solidification Front During Upwards Solidification," *Journal of Fluid Mechanics*, Vol. 204, July 1989, pp. 581-597.
- ⁷Trivedi, R., Han, S. H., and Sekhar, J. A., "Microstructural Development in Interfiber Regions of Directionally Solidified Composites," *Solidification of Metal-Matrix Composites*, edited by P. K. Rohatgi, The Metallurgical Society of the American Institute of Mining, Metallurgical and Petroleum Engineers (AIME), Warrendale, PA, 1990, pp. 23-37.
- ⁸Cerisier, P., Perez-Garcia, C., Jamond, C., and Pantaloni, J., "A New Experimental Method to Select Hexagonal Patterns in Bénard-Marangoni Convection," *Physics Letters A*, Vol. 112, Nov. 1985, pp. 366-370.
- ⁹Billia, B., Jamgotchian, H., Favier, J. J., and Camel, D., "Solidification Cellulaire d'Alliages Pb-Tl lors de l'Expérience D1-WL-GHF-02," *Proceedings of the 6th European Symposium on Materials Sciences Under Microgravity Conditions*, European Space Agency-SP 256, Noordwijk, The Netherlands, Feb. 1987, pp. 377-382.
- ¹⁰Jamgotchian, H., Trivedi, R., and Billia, B., "An Array of Doubles: a Branch of Cellular Solutions in Directional Solidification," *Physical Review E* (to be published).
- ¹¹Jamgotchian, H., Trivedi, R., and Billia, B., "Interface Dynamics and Coupled Growth in Directional Solidification in Presence of Bubbles," *Journal of Crystal Growth* (submitted for publication).
- ¹²Misbah, C., Müller-Krumbhaar, H., and Saito, Y., "Dendritic Growth and Directional Solidification," *Journal of Crystal Growth*, Vol. 99, Nos. 1-4, 1990, pp. 156-160.
- ¹³Cerisier, P., Occelli, R., Perez-Garcia, C., and Jamond, C., "Structural Disorder in Bénard-Marangoni Convection," *Journal de Physique (France)*, Vol. 48, April 1987, pp. 569-576.

Modern Engineering for Design of Liquid-Propellant Rocket Engines

Dieter K. Huzel and David H. Huang

From the component design, to the subsystem design, to the engine systems design, engine development and flight-vehicle application, this "how-to" text bridges the gap between basic physical and design principles and actual rocket-engine design as it's done in industry. A "must-read" for advanced students and engineers active in all phases of engine systems design, development, and application, in industry and government agencies.

Chapters: Introduction to Liquid-Propellant Rocket Engines, Engine Requirements and Preliminary Design Analyses, Introduction to Sample Calculations, Design of Thrust Chambers and Other Combustion Devices, Design of Gas-Pressurized Propellant Feed Systems, Design of Turbopump Propellant Feed Sys-

tems, Design of Rocket-Engine Control and Condition-Monitoring Systems, Design of Propellant Tanks, Design of Interconnecting Components and Mounts, Engine Systems Design Integration, Design of Liquid-Propellant Space Engines PLUS: Weight Considerations, Reliability Considerations, Rocket Engine Materials Appendices, 420 illustrations, 54 tables, list of acronyms and detailed subject index.

AIAA Progress in Astronautics and Aeronautics Series

1992, 431 pp, illus ISBN 1-56347-013-6

AIAA Members \$89.95 Nonmembers \$109.95 Order #: V-147

Place your order today! Call 1-800/682-AIAA



American Institute of Aeronautics and Astronautics

Publications Customer Service, 9 Jay Gould Ct., P.O. Box 753, Waldorf, MD 20604
FAX 301/843-0159 Phone 1-800/682-2422 9 a.m. - 5 p.m. Eastern

Sales Tax: CA residents, 8.25%; DC, 6%. For shipping and handling add \$4.75 for 1-4 books (call for rates for higher quantities). Orders under \$100.00 must be prepaid. Foreign orders must be prepaid and include a \$20.00 postal surcharge. Please allow 4 weeks for delivery. Prices are subject to change without notice. Returns will be accepted within 30 days. Non-U.S. residents are responsible for payment of any taxes required by their government.